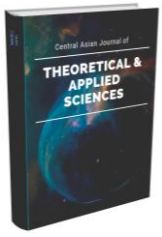

CENTRAL ASIAN JOURNAL OF THEORETICAL AND APPLIED SCIENCE

https://cajotas.centralasianstudies.org/index.php/CAJOTAS
Volume: 06 Issue: 04 | October 2025 ISSN: 2660-5317

Article

Design, Synthesis, Characterization, and Biological Evaluation of Novel Isatin-Based Mannich Derivatives with Antibacterial and Anticancer Activities

Hussein A Hamzah[1], Shahad M. Hussain[2], Aqeel Mohamed[3], Abbas K. Abbas[4]

1. Chemistry Department, College of Science, Al-Nahrain University, Baghdad, Iraq
2. Medical Physics Department, College of Science, Al-Nahrain University, Baghdad, Iraq
3. Department of Medical Lab Technique, Sawa University, Muthanna, Iraq
4. Muthana Agriculture Directorate, Ministry of Agriculture, Al-Muthana, Iraq

*Correspondence: hussein.ali@nahrainuniv.edu.iq, Shahad.muhammed@nahrainuniv.edu.iq, aqeelmohammed@sawauniversity.edu.iq, Abbaschemist1991@gmail.com

Abstract: Mannich base derivatives have emerged as promising scaffolds in medicinal chemistry due to their structural versatility and broad-spectrum biological activities. This study reports the synthesis and characterization of two novel Mannich base derivatives (S1 and S2) derived from isatin, formaldehyde, and substituted aniline derivatives via a one-pot condensation reaction. The synthesized compounds were confirmed using FTIR and ^{1}H-NMR spectroscopy, indicating successful β-amino ketone formation. The antimicrobial efficacy of S1 and S2 was assessed against *Staphylococcus aureus* and *Escherichia coli* using the cup-plate agar diffusion method at three concentrations. Results revealed dose-dependent inhibition, with S2 showing enhanced activity likely due to its hydroxyl group. Both compounds were tested for cytotoxic capability against MCF-7 human breast cancer cells. S1 showed better anticancer efficacy with a lower IC_{50} value (~36.9 ppm) than S2 (~41.2 ppm). Both compounds bound well to the oestrogen receptor alpha (PDB ID: 5T92) in molecular docking tests using MOE software. Compound A1 (derived from S2) showed significant hydrogen bonding and π-interactions with critical residues, indicating medicinal potential. Synthesis, spectroscopy, biological tests, and computer docking give a comprehensive knowledge of structure–activity interactions, supporting Mannich derivatives as dual-action medicines. To clinically translate these drugs, mechanistic research and in vivo assessment are needed.

Keywords: Antibacterial, Anticancer, Estrogen receptor, Mannich base, Molecular docking.

Citation: Hamzah, H. A & Hussain, S. M & Mohamed, A & Abbas, A. K. Design, Synthesis, Characterization, and Biological Evaluation of Novel Isatin-Based Mannich Derivatives with Antibacterial and Anticancer Activities. Central Asian Journal of Theoretical and Applied Science 2025, 6(4), 689-704.

Received: 10th May 2025
Revised: 16th Jun 2025
Accepted: 24th Jul 2025
Published: 12th Aug 2025

1. Introduction

As drug-resistant microbial strains arise and cancer rates grow worldwide, innovative therapeutic agents with improved effectiveness and selectivity are needed. Due to their biological versatility, structural flexibility, and synthetic accessibility, Mannich base derivatives have garnered interest in pharmaceutical and medical chemistry [1], [2]. In 1912, Carl Mannich described the Mannich reaction, which condenses an aldehyde (usually formaldehyde), an amine, and an active hydrogen molecule to generate β-amino carbonyl compounds called Mannich bases. These chemicals are essential organic synthesis intermediates and drug development pharmacophores [3], [4].

Mannich bases have been investigated for decades for their antibacterial, antifungal, anticancer, anti-inflammatory, anticonvulsant, and analgesic properties. Their biological potential comes from the β-amino ketone group, which enhances lipophilicity, membrane penetration, and drug absorption [5]. Adding hydroxyl, methoxy, halogen, or heterocyclic

substituents may enhance these compounds' pharmacological and pharmacokinetic characteristics. Recent research reveal that Mannich bases containing phenolic or aromatic amines may kill breast (MCF-7), lung (A549), and colon (HT-29) cancer cell lines by apoptosis, DNA intercalation, or topoisomerase and kinase inhibition Mannich compounds kill Gram-positive and Gram-negative bacteria at wide spectru [6]. These molecules' aromatic ring systems' electron-donating or electron-withdrawing groups impact electronic density and target binding affinity, influencing antibacterial action. Antibacterial and anticancer characteristics make Mannich bases with isatin scaffolds attractive. Isatin, an indole derivative, is useful in medicinal chemistry because to its ability to form hydrogen bonds and π-π stacking interactions with enzyme active sites and DNA grooves .

Mannich base derivatives are common yet have gaps. Many studies do preliminary biological evaluations without mechanistic or dose–response analysis. Few studies compare the biological activity with methyl and hydroxyl substituents [7]. When developing multifunctional cancer drugs for immunocompromised individuals, structural features must match antibacterial and anticancer activity. To solve these deficiencies, novel Mannich derivatives must be synthesized, structurally characterized, and physiologically assessed [8].

This work synthesizes and biomedically evaluates two new Mannich base derivatives, S1 and S2, from the one-pot reaction of isatin, formaldehyde, and substituted aromatic amines. S1 relies on N,4-dimethylaniline, whereas S2 uses N-methyl-4-hydroxylaniline, enabling comparison of electron-donating methyl and hydroxyl functionalities on bioactivity. Synthesized derivatives undergo structural characterization using FTIR and ^{1}H-NMR to confirm β-amino ketone connections.

In addition, S1 and S2 are tested against MCF-7 at 20–320 ppm for cytotoxicity. To quantify drug potency, conventional in vitro tests monitor cell viability and dose-response curves are used to obtain IC_{50} values. This research uses structural analysis and antibacterial and anticancer assessments to evaluate structure–activity connections and if particular substituents improve therapeutic potential. This finding should help rationally develop next-generation Mannich-based antibacterial and anticancer drugs [9].

2. Materials and Methods

Materials

All chemicals and reagents in this investigation were analytical-grade and unpurified. Isatin (1H-indole-2,3-dione), formaldehyde solution (37% w/w in water), N,4-dimethylaniline, and N-methyl-4-hydroxylaniline were obtained from Sigma-Aldrich (Germany). Tetrahydrofuran (THF), dimethyl sulfoxide (DMSO), and cold distilled water were purchased from Merck (Germany) and used as received. Ceftriaxone (standard antibacterial drug) was obtained from a certified pharmaceutical supplier.

Methodology

1. Synthesis of Mannich Derivatives (S1 and S2)

The Mannich base derivatives **S1** and **S2** were synthesized through a classical one-pot, three-component condensation reaction involving equimolar quantities of isatin, formaldehyde, and substituted aromatic amines. In a standard experimental procedure, isatin (3.52 g, 0.02 mol) dissolved in 15 mL of tetrahydrofuran (THF) and subjected to continuous magnetic stirring at room temperature. Two parallel reactions were conducted to obtain the respective derivatives, differing only in the amine precursor employed. For the synthesis of **S1**, N,4-dimethylaniline (0.02 mol) was introduced into the reaction system, whereas for **S2**, N-methyl-4-hydroxylaniline (0.02 mol) was added under identical conditions, as depicted in *Scheme 1*.

Upon complete homogenization of the amine substrates, 12 mL of aqueous formaldehyde solution (37% w/w) was added dropwise to each reaction mixture with continuous stirring to ensure uniform dispersion and initiation of the condensation

process. The mixtures were subsequently stirred at ambient temperature for one hour, followed by gentle reflux on a steam bath for 20 min to promote product formation. After thermal treatment, after cooling to room temperature, the mixes were kept at 4 °C for 48 h to crystallize. The resulting crystalline products, corresponding to S1 and S2, were collected by vacuum filtration, thoroughly washed with cold distilled water to remove unreacted residues, and subjected to further purification to obtain the final pure compounds.

The physicochemical properties of derivative S1: Molecular weight is 280.327, molecular formula $C_{17}H_{16}N_2O_2$, yield% 72, and light-yellow color. While derivative S2: Molecular weight is 282.299, molecular formula $C_{16}H_{14}N_2O_3$, yield% 68, and yellow color.

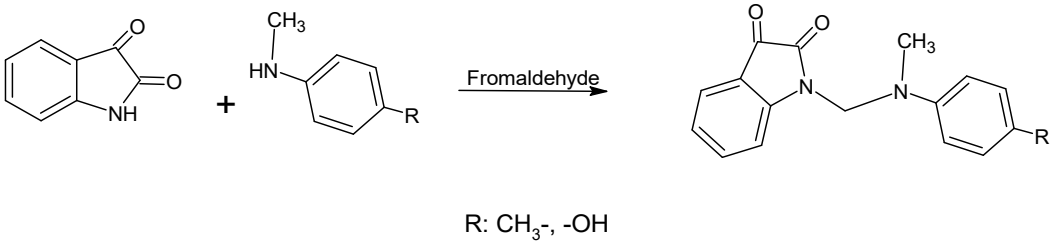

R: CH_3-, -OH

Scheme 1. Routes of synthesized Mannich derivatives S1 and S2.

2. Investigation of the Antimicrobial Activity of Synthesized Derivates (S1 and S2)

The synthesized Mannich base derivatives S1 and S2 were tested for antibacterial activity utilizing cup-plate agar diffusion and millimeter-measured inhibitory zones. These compounds were evaluated at 0.1, 0.001, and 0.00001 mg/mL with ceftriaxone as the reference medication. Antibacterial efficacy was assessed against two clinically relevant bacterial strains, *Staphylococcus aureus* and *Escherichia coli*, isolated from various clinical sources such as infected wounds, nasal swabs, urinary tract infections, and surgical specimens. Muller-Hinton agar served as the culture medium, which was sterilized, poured into sterile Petri dishes, and allowed to solidify under aseptic conditions. Bacterial suspensions were evenly spread over the agar surface using a sterile triangular loop, after which stainless steel cylinders (12 mm diameter) were positioned on the agar to create wells. The synthesized compounds, dissolved in dimethyl sulfoxide (DMSO), were introduced into the wells at the designated concentrations, while the standard drug was prepared in sterile distilled water. After one hour at room temperature for pre-diffusion, the plates were incubated at 37 °C for 48 hours. The antibacterial potential of the synthesized derivatives was determined by measuring the inhibitory zone diameters in millimeters after incubation [10].

3. Molecules Library Preparation

ChemDraw Ultra 12.0 (https://chemdraw pro.software.informer.com/12.0/) was used to construct the 3D structures of the freshly synthesized chemical (S2) and to minimize its energy for molecular docking (10). Using Hyperchem 8.08, semi-empirical AM1 pre-optimized the structures. DFT optimized the structures for the most stable conformation using the B3LYP/6-31G basis set (10). Maximum force, RMS force, displacement, and displacement converge to "YES" by default. All ligand vibrational frequency measurements are positive, suggesting stability. To assess ligand affinity, MOE software (Molecular Operating Environment (MOE), 2019) integrated the optimized structures into one database (Scheme 2) and (Scheme 3). Scheme 1 shows the docking, ligand analysis, and reactivity process schematically [11].

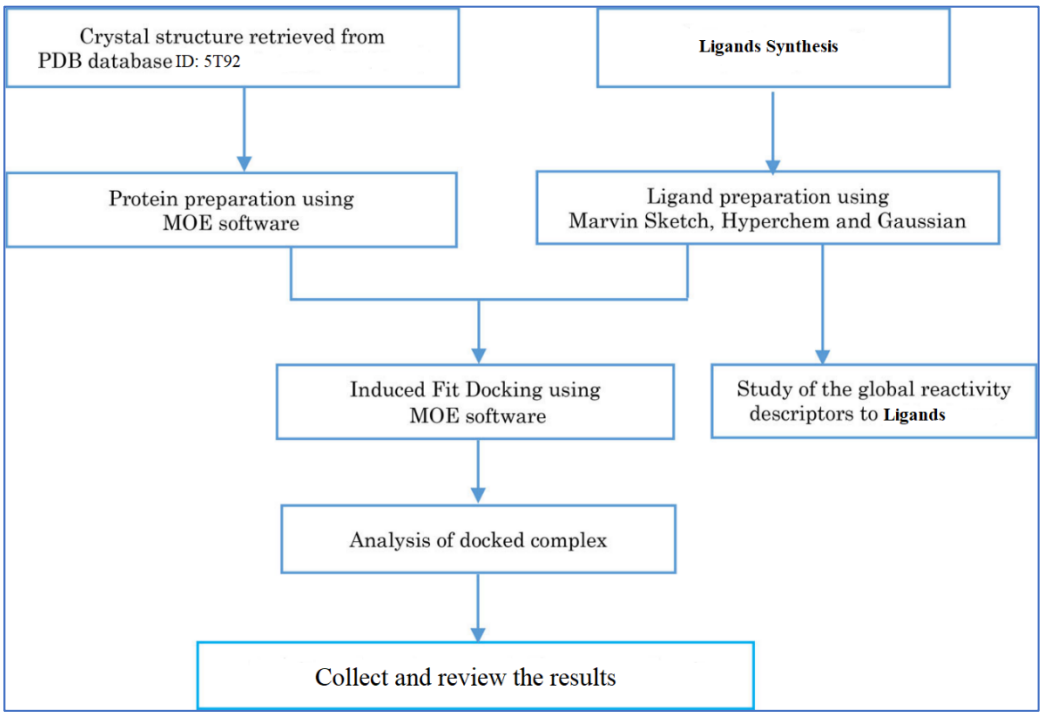

Scheme 2. Schematic of docking, ligand analysis, and reactivity.

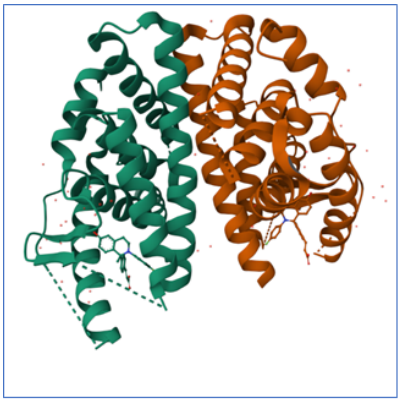

Crystal structures of the 5T92 protein

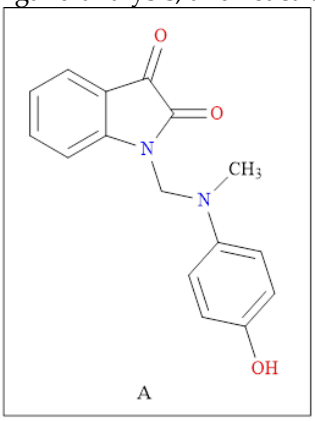

2D structure of selected compound (ligand).

Scheme 3. 2D structure of selected compound (ligand).

4. Receptor Preparation

The crystal structure of the Oestrogen receptor alpha ligand binding domain in complex with (2E) was chosen from the Protein Data Bank (PDB ID: 5T92).-3-{4-[(1R)-2-(4-fluorophenyl)6-hydroxy-1-methy l-1,2,3,4-tetrahydroisoquinolin-1-yl]phenyl-prop-2-enoic The target enzyme's active site water molecule is essential, thus it was inserted to link the ligand and target hydrogenally. Repairing X-ray diffraction-broken links and adding hydrogen atoms created the protein structure [12]. Importantly, PDB is a reliable source for biological macromolecule crystal structures globally, as shown in Scheme 2.

The Oestrogen Receptor alpha (ERα) ligand-binding domain, 5T92, is critical for the development and progression of oestrogen receptor-positive (ER^+) breast cancer. When ERα binds to oestrogen, it activates genes involved in cell growth and survival. In hormone-dependent breast cancer, ERα overexpression or activation leads to uncontrolled cell proliferation, making it a crucial therapeutic target. A well-characterized binding location and importance to hormone-driven breast cancer led to its selection for molecular docking, enabling in silico screening of putative ERα antagonists [13].

5. Ligand-Protein Molecular Docking

MOE was used for all docking and scoring computations (Molecular Operating Environment, 2019). Oestrogen receptor alpha ligand binding domain crystal structure in combination with (2E)-3-{4-[(1R)]-2-(4-fluorophenyl)-6-hydroxy-1-methyl-1,2,3,4-tetrahydroisoquinolin-1-yl]phenyl-prop-2-enoic acid (PDB ID: 5T92) (Scheme 2), retrieved from the Protein Data Bank at 2.22 Å resolution. A resolution of 1.5 to 2.5 Å is suitable for docking investigations. The optimal RMSD score is about 2 Å with an energy score below -7 kcal/mol. These two values are typically used to confirm molecular docking results.

3. Results and Discussion

Characterization

The Mannich reaction in this study begins with the formation of a reactive iminium ion. The substituted aromatic amine, either N,4-dimethylaniline (for S1) or N-methyl-4-hydroxylaniline (for S2), reacts with aqueous formaldehyde under mild stirring conditions. Initially, the amine nucleophilically attacks the electrophilic carbon of formaldehyde, producing a carbinolamine intermediate. This intermediate subsequently undergoes dehydration, releasing a molecule of water and generating a highly electrophilic iminium ion ($R–NH^+=CH_2$), which serves as the key reactive species in the condensation process. In the second stage, isatin acts as the nucleophilic component. The C-3 position of isatin, adjacent to the carbonyl group, is activated due to the electron-withdrawing nature of the carbonyl moieties, which increases the acidity of the α-proton and facilitates nucleophilic attack. The electron-rich carbon at this position attacks the electrophilic carbon of the iminium ion, resulting in the formation of a new C–C bond. This step leads to the generation of a β-amino ketone intermediate, a hallmark structure in Mannich base derivatives. The reaction conditions, including gentle reflux, ensure sufficient energy for bond formation while minimizing side reactions.

Finally, the product formation and crystallization occur as the reaction mixture is cooled and stored at a low temperature. Proton rearrangements stabilize the β-amino ketone framework, and the Mannich base derivatives S1 and S2 precipitate due to their low solubility in the reaction medium. The crude products are collected by vacuum filtration, washed thoroughly to remove unreacted materials and by-products, and further purified to yield the final crystalline Mannich bases. This sequence effectively demonstrates the classical one-pot three-component Mannich condensation, producing β-amino ketone derivatives in good yield and purity [14].

The FTIR (cm^{-1}) spectrum of the synthesized derivative S1 is shown in Figure 1. The C-H of the aliphatic chain at 2992 and the C-H aromatic at 3062, the carbonyl group at 1712, the C=C of the aromatic ring at 1615, and the C-N shows at 1074. ^{1}H-NMR (ppm) showed Figure 3 for derivative S1, several signals as (m, 10H, protons aromatic ring) at 6.80-7.79, and methylene groups showed as singlet signals at 4.94, the methyl group that linked to the nitrogen atom showed at 3.16, and the methyl group showed as a singlet signal at 2.15 [14], [15].

The FTIR (cm^{-1}) spectrum of the synthesized derivative S2 is shown in Figure 2. The hydroxyl group shows as a broad peak at 3368, the C-H of the aliphatic chain at 2981, the carbonyl group at 1711, the C=C of the aromatic ring at 1609, and the C-N shows at 1053. ^{1}H-NMR (ppm) showed Figure 4 for derivative S2, (S, OH, 1H) of protons of hydroxyl groups appeared at 9.73 several signals as (m, 10H, protons aromatic ring) at 7.04-7.92, and methylene groups showed as singlet signals at 4.90, and the methyl group that linked to the nitrogen atom showed at 3.01[16], [17].

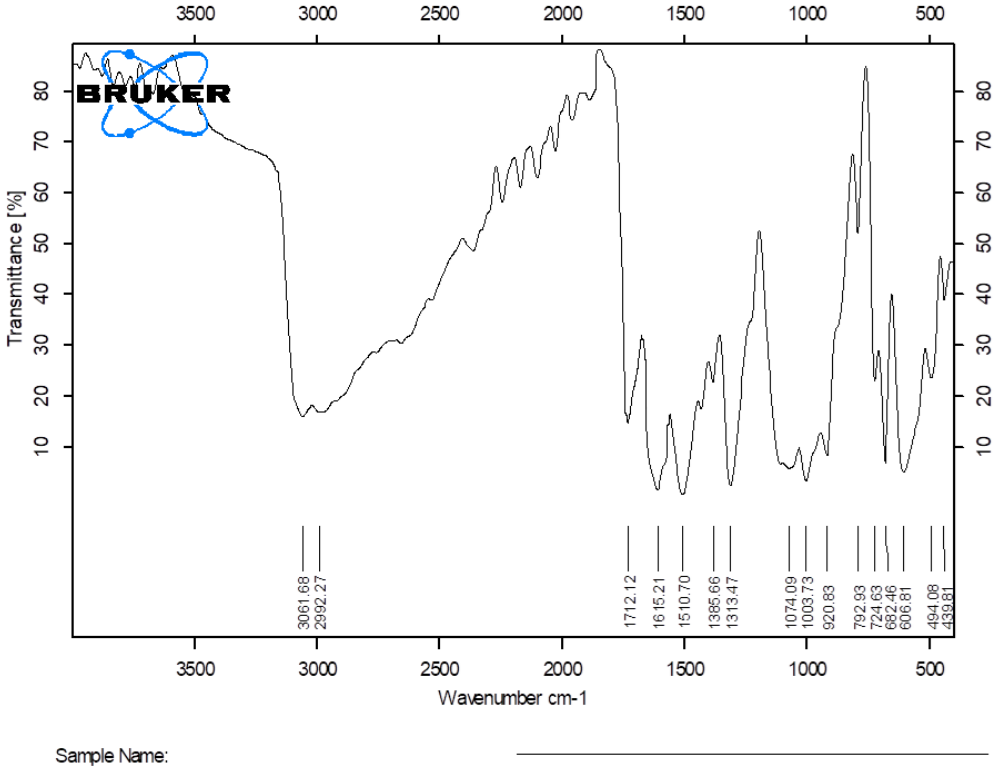

Figure 1. FTIR spectrum of derivative S1.

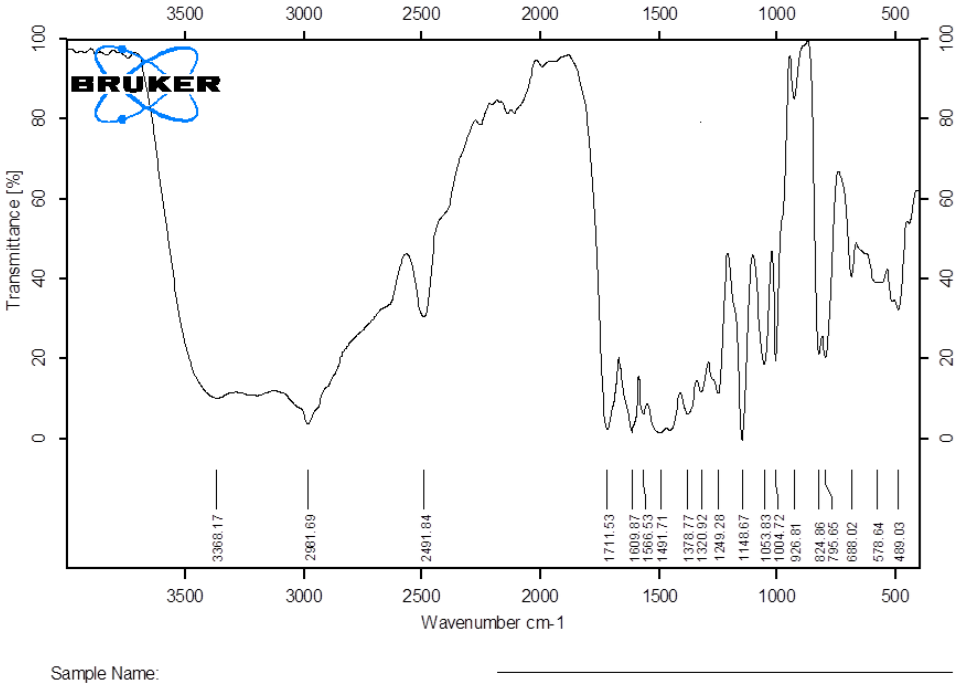

Figure 2. FTIR spectrum of derivative S2.

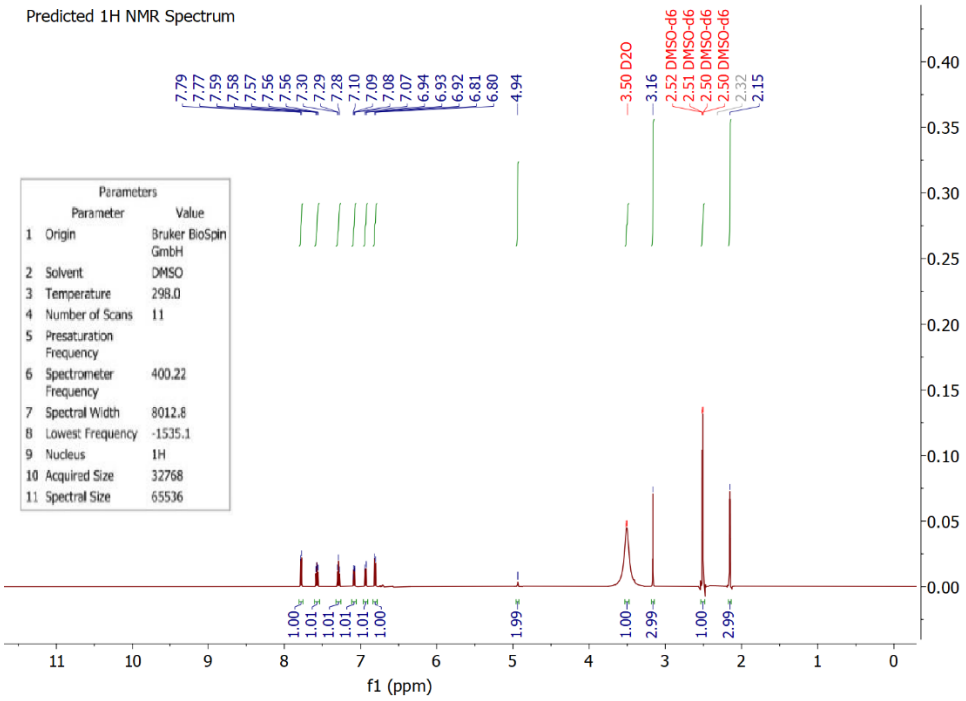

Figure 3. [1]H-NMR spectrum of derivative S1.

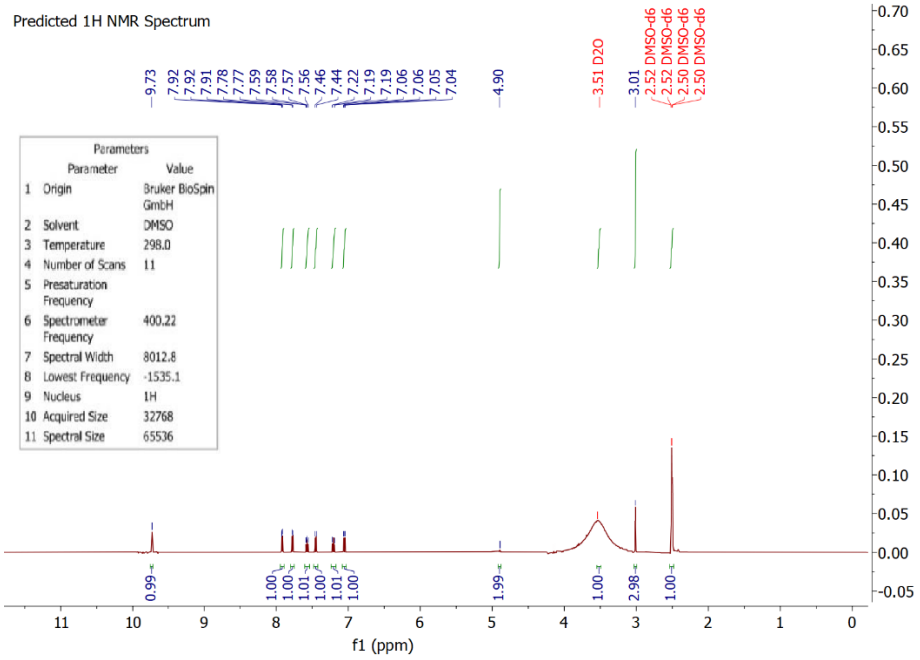

Figure 4. [1]H-NMR spectrum of derivative S2.

Applications

Biological Activity: The antibacterial evaluation of the synthesized Mannich base derivatives S1 and S2 demonstrates that both compounds possess inhibitory activity against *Staphylococcus aureus* and Escherichia coli, with the magnitude of inhibition being concentration-dependent. At the highest tested concentration (0.1 mg/mL), S2 exhibits superior antibacterial efficacy compared to S1, producing inhibition zones of 23 mm against *S. aureus* and 18 mm against *E. coli*, whereas S1 produces zones of 18 mm and 15 mm, respectively. The higher activity of S2 may be attributed to the presence of the hydroxyl group on the aromatic ring, which can enhance hydrogen bonding interactions with bacterial enzymes or cell wall components, thereby improving antimicrobial potency. (Figure 4) Conversely, S1, bearing two methyl substituents, may display slightly reduced activity due to steric hindrance that limits interaction with the target sites [15], [16].

The decrease in inhibition zones at lower doses (0.01, 0.001 and 0.00001 mg/mL) for both derivatives shows that their antimicrobial effect is dose-dependent, indicating that active compounds directly affect bacterial growth. Both chemicals work better against S. aureus than E. coli, perhaps due to Gram-positive and Gram-negative cell wall structural variations. Gram-negative bacteria's outer membrane may operate as a permeability barrier, decreasing chemical diffusion and buildup at the site of action. These findings are consistent with previous studies reporting enhanced antimicrobial activity of Mannich base derivatives containing phenolic or hydroxyl substituents, which improve lipophilicity and binding affinity to bacterial proteins according to Rimpiläinen, Tatu, et al . Rimpiläinen, T reported similar structure–activity relationships, where phenolic Mannich bases showed increased potency against Gram-positive strains . The results obtained here reinforce the potential of Mannich base scaffolds as promising antibacterial agents and suggest that further structural modifications, particularly involving electron-donating groups capable of hydrogen bonding, could enhance their biological activity spectrum and potency (Figure 5)

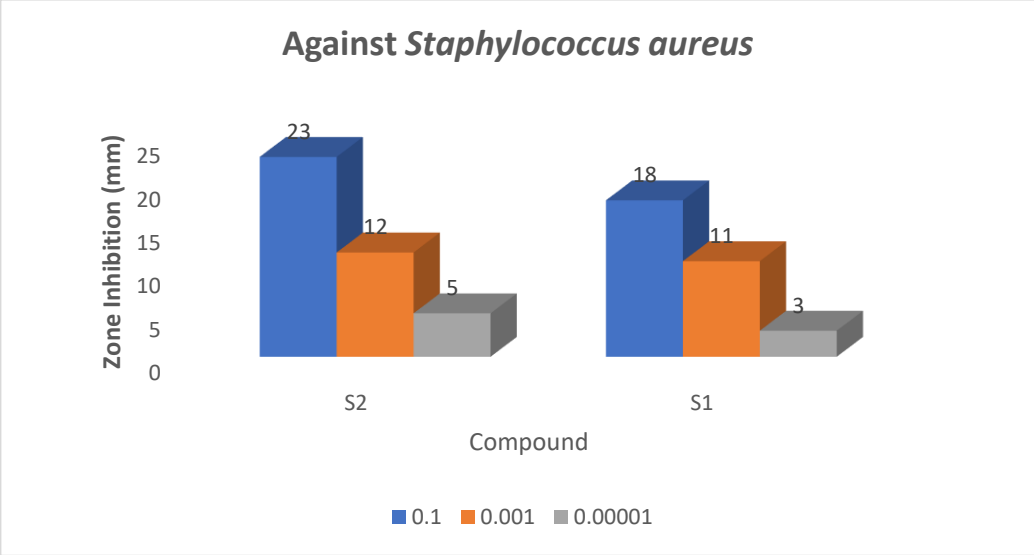

Figure 5. Biological activity of synthesized derivatives S1 and S2 against *Staphylococcus aureus*.

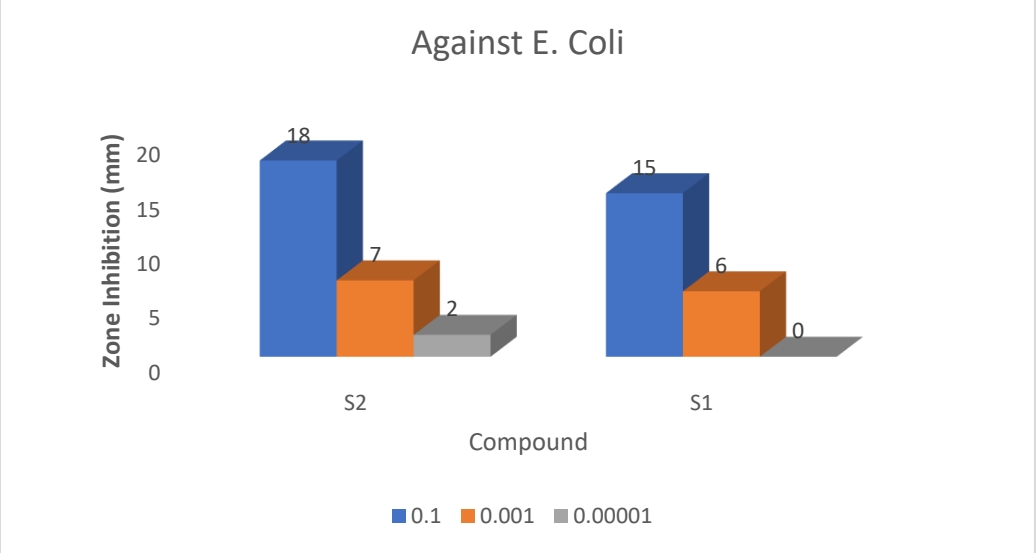

Figure 6. Biological activity of synthesized derivatives S1 and S2 against *E. Coli*.

Anti-Breast Cancer MCF-7 Cell Line:

Both Mannich derivatives (S1 and S2) suppress MCF-7 viability in a concentration-dependent fashion across 20–320 ppm. Mean viability falls monotonically with dose, reaching ~6.8% (S1) and ~10.1% (S2) at 320 ppm, which is consistent with a predominantly

cytotoxic effect rather than mere growth arrest. Nonlinear regression of the dose–response data (four-parameter logistic model) yields IC_{50} values of ~36.9 ppm for S1 and ~41.2 ppm for S2, indicating that S1 is modestly more potent overall. The steeper slope for S1 at ≥80 ppm suggests more efficient intracellular accumulation and/or engagement of critical death pathways at higher exposure, whereas S2 displays a shallower decline and higher residual viability at the top dose, as shown in Tables 1 and 2.

Structure-activity considerations plausibly account for these differences. S1 carries two methyl substituents on the aniline ring, which increase lipophilicity and can enhance passive diffusion across cellular membranes, thereby elevating effective intracellular concentration and apparent potency. S2 contains a phenolic OH that can participate in hydrogen bonding with biomolecular targets, but partial ionization at physiological pH may reduce membrane permeability and flatten the dose–response [17], [18]. Notably, S2 tends to perform comparatively better at the lowest dose (20 ppm), which could reflect early target engagement via polar interactions; however, the potency advantage shifts to S1 as dose increases, pointing to transport and exposure as key determinants at higher concentrations. These mechanistic inferences require validation by uptake assays and target-engagement studies.

Table 1. Cytotoxic effect of synthesized S1 on MCF-7 Cell Line.

Concentration	Mean	∓ SD
0 ppm	100.056	1.866
20 ppm	65.427	1.390
40 ppm	49.266	3.518
80 ppm	28.604	2.742
160 ppm	17.576	1.202
320 ppm	6.795	0.777

Table 2. Cytotoxic effect of synthesized S2 on MCF-7 Cell Line.

Concentration	Mean	∓ SD
0 ppm	100.208	1.600
20 ppm	60.262	2.801
40 ppm	51.436	2.320
80 ppm	41.348	1.798
160 ppm	27.289	0.685
320 ppm	10.137	1.401

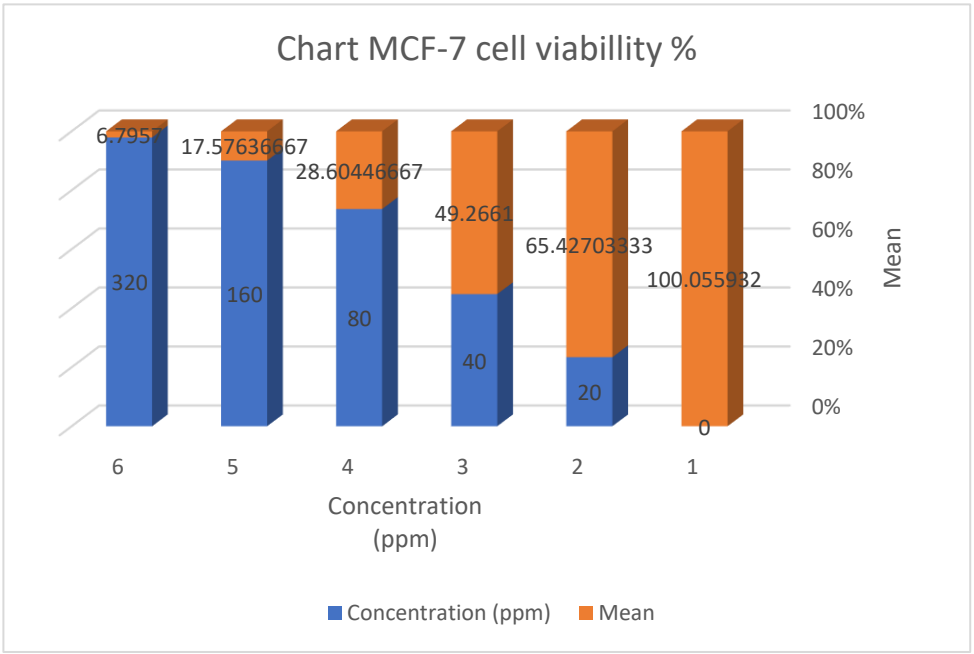

Figure 7. Effect of S1 treatment on viable cell count in MCF-7.

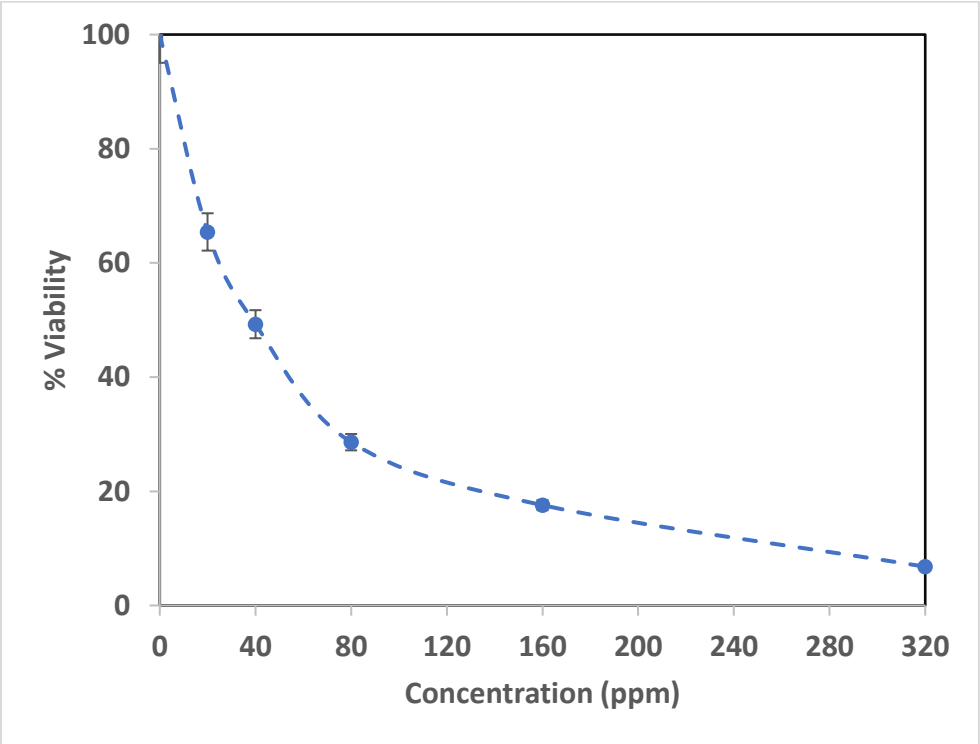

Figure 8. Cytotoxic effect of S1 against MC-F-7.

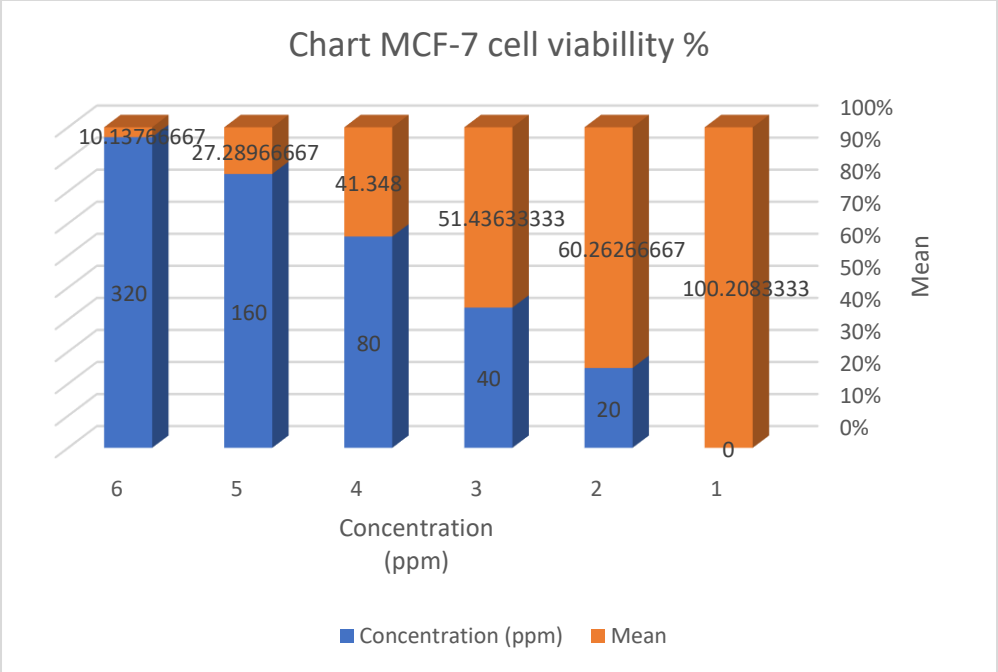

Figure 9. Effect of S2 treatment on viable cell count in MCF-7.

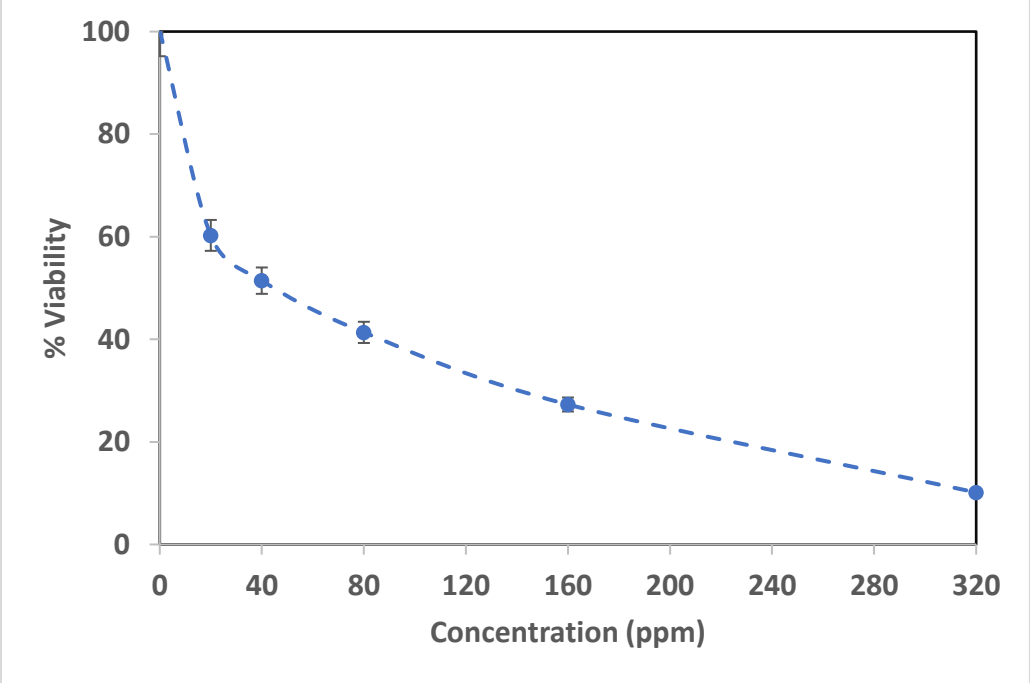

Figure 10. Cytotoxic effect of S2 against MC-F-7.

Molecular Docking Study: Molecular docking is used as a fundamental tool in the drug discovery pipeline. In the present study, MOE software was applied to perform all molecular docking calculations and predict the binding modes of the prepared compound (S2) with the protein (5T92), see Figure 3. The predicted binding affinities and features of the investigated compound (S2) towards (5T92) are listed in Table 2 and 3 shows the best binding poses of compound (S2) against target protein.

The 2D and 3D representations of interactions of the inspected compounds with the key amino acid residues of the (5T92) protein are illustrated in the following figures and tables. Compound (S2) showed good binding affinity values, as shown in Tables 4 and 5, with protein (PDB ID: 5T92). The binding and mode of interactions of the compound (S2) with the (PDB ID: 5T92) protein are shown in 2D and 3D figure 9. From the interactions, it has been demonstrated that primarily there are different types of interactions (hydrogen bonding and hydrophobic interactions). Interactions were further examined for bond lengths and hydrogen bonds in the active site and were illustrated in the following figures. The results from these figures showed that compound (S2) interacts with different amino acid residues in different interactions: H-donor, H-acceptor, and H-pi, as well as two H-acceptor and pi-H interactions with the water and other amino acids. The distance and energy binding of the interaction are listed in Table 3.

Table 3. The binding affinity and Rmsd result of 5T92 protein from docking process.

Compounds	mseq	Binding Affinity Kcal/mol	Rmsd (Å)	E_conf	E_place	E_score1	E_refine	E_score2
A1	1	-7.39337	2.128035	15.1202	-10.6596	-12.4975	-32.6579	-7.39337
A2	1	-7.18311	1.089393	17.07996	-11.8302	-12.8499	-29.5219	-7.18311
A3	1	-6.56082	1.22176	14.48386	-11.7992	-12.1505	-30.4363	-6.56082

A4	1	-6.48321	1.58274	15.06902	-12.2823	-13.1149	-32.1518	-6.48321
A5	1	-6.42785	1.081642	13.99143	-13.2084	-12.3178	-32.001	-6.42785
Standard	std	-7.91706	2.137427	-93.9605	-102.304	-11.9107	-36.5557	-7.91706

Table 4. Smiles of selected ligand.

Compounds	Binding Affinity Kcal/mol	Rmsd (Å)
A1	-7.39337	2.128035
A2	-7.18311	1.089393
A3	-6.56082	1.22176
A4	-6.48321	1.58274
A5	-6.42785	1.081642
Standard	-7.91706	2.137427

Table 5. Details of the best pose of ligand (S2) with protein 5T92.

Compounds	Binding Affinity Kcal/mol	Rmsd (Å)	Atom of compound	Atom of Receptor	Involved receptor residues	Type of interaction bond	Distance (Å)	E (kcal/mol)
A1	-7.39337	2.128035	O 2 O 2 6-ring 6-ring	OE1 NH2 CB CD1	GLU 353 ARG 394 LEU 387 PHE 404	(A) H-donor (A) H-acceptor (A) pi-H (A) pi-H	2.67 2.87 4.43 4.11	-4.8 -0.7 -0.4 -0.6
Standard	-7.91706	2.137427	O11 47 6-ring 6-ring 6-ring	OE1 CB CD1 CE	GLU 353 ALA 350 PHE 404 MET 421	(A) H-donor (A) pi-H (A) pi-H (A) pi-H	2.53 4.66 4.14 4.25	-3.8 -0.5 -0.4 -0.3

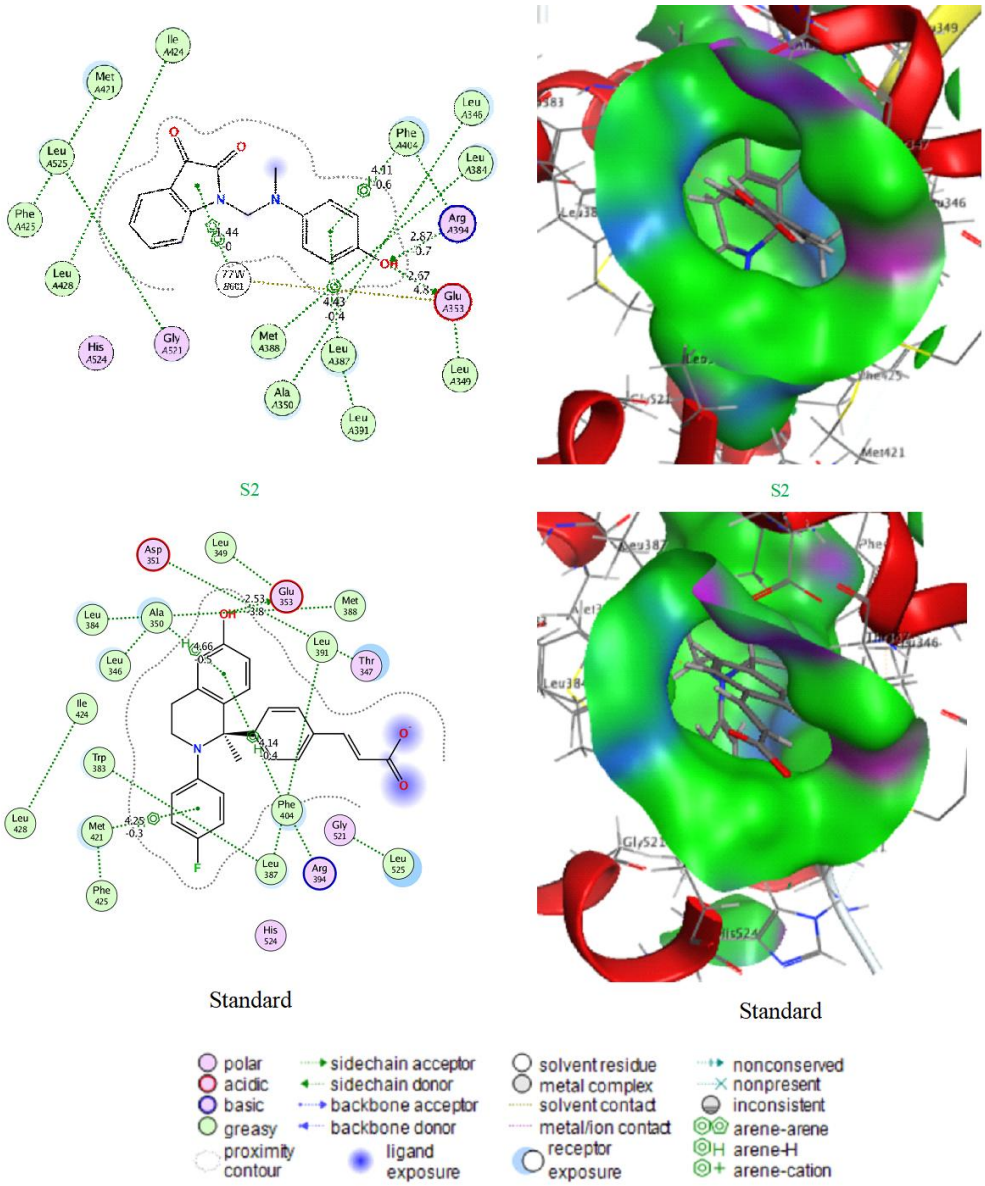

Figure 11. 2D and 3D of the best poses.

Interpreting Molecular Docking Findings

The preceding tables provide a complete understanding of the compounds' docking data against the 5T92 protein. (Figure 9) The first table compares the protein's binding interactions with the top-performing ligand, A1, to the standard molecule. The binding affinity of A1 is -7.39337 kcal/mol, which is slightly less negative than the standard compound's affinity of -7.91706 kcal/mol, indicating that the standard has slightly stronger binding. However, values below -6 indicate significant binding strength, so A1 still has good affinity. A1 has a steady binding conformation with an RMSD value of 2.128035 Å, identical to the standard's 2.137427 Å, indicating a consistent binding posture. A1 creates strong hydrogen bonds with GLU 353 at 2.67 Å and ARG 394 at 2.87 Å, stabilising the ligand in the binding site. Moreover, A1 engages in pi-H interactions with LEU 387 and PHE 404 at 4.43 Å and 4.11 Å, respectively, promoting overall stability via hydrophobic and aromatic interactions. These bonds have interaction energies (E) of -0.7 to -0.4 kcal/mol, except for the H-donor interaction with GLU 353, which is more favorable at -4.8 kcal/mol, suggesting that this bond is a key contribution to A1 stabilization in the binding pocket. The standard's hydrogen bonding and pi-H interactions with critical residues are similar, although the most energetically favourable hydrogen bond (with GLU 353) is

somewhat less negative at -3.8 kcal/mol, while the other interactions are similar. This shows that both drugs bind to critical amino acids in the protein's active site in similar binding conditions.

The first table, which summarizes docking scores and energy terms for all compounds, shows that A1 outperforms A2 to A5 across all energy measures. Except for the standard, which has the worst binding affinity, A1 has the best. This confirms its standing as the reference molecule. RMSD values of A1 and other ligands range from 1 to 2 Å, demonstrating solid docking solutions and poses. The extra energy terms E_conf, E_place, E_score1, E_refine, and E_score2 illuminate the docking process. A1's E_conf value of 15.1202 suggests a favourable conformational energy, while its E_place and E_score1 values of -10.6596 and -12.4975 indicate good binding pocket placement and initial scoring. The ligand-protein combination is stable after energy minimization, as shown by the optimized interaction energy E_refine score of -32.6579. E_score2, which reassesses binding affinity after complete docking, indicates that A1 maintains its robust binding properties following refinement, in all conformational and contact energies, A2 through A5 exhibit lower binding affinities than the other chemicals. Despite its highest binding affinity, the standard has substantially negative E_conf and E_place values, which may indicate a superior protein-binding pocket interaction. Overall, A1 is the most promising ligand, nearly matching the binding performance of the reference molecule and generating several stabilizing contacts with 5T92 protein residues. A1's and the standard's strong hydrogen bonding and pi-H interactions reveal comparable binding stabilization processes, confirming its dependability and promise as a lead chemical for future study.

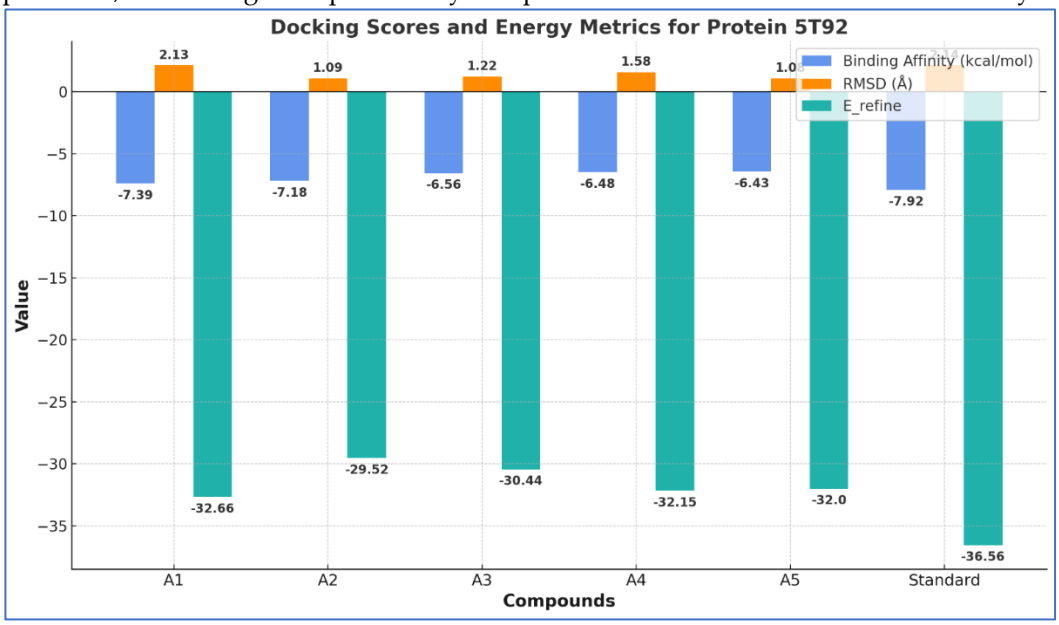

Figure 12. A detailed and professionally structured bar chart compares docking results for compound A1.

A detailed and professionally structured bar chart compares docking results for compounds A1, A2, A3, A4, A5, and a Standard ligand against the target protein 5T92. (Figure 10) Three crucial docking metrics are clearly provided for each compound: Binding Affinity (kcal/mol), Root Mean Square Deviation (RMSD, Å), and refined energy (E_refine). The binding affinity bars (blue) show the intensity of each ligand-protein interaction, with negative values suggesting stronger interactions. The Standard ligand has the highest affinity at -7.92 kcal/mol, followed by compound A1 at -7.39. Lower RMSD values (orange bars) imply improved docking accuracy and posture dependability for the ligand. All compounds had acceptable RMSD values, especially compounds A2, A3, and A5, indicating stable protein binding conformations. The E_refine bars (green) show the refined interaction energies after additional optimisation, with larger negative values indicating more stability and better binding site interactions. The Standard compound has

the best E_refine score at -36.56, followed by A1, A4, and A5. The given chart is detailed and straightforward enough for scientific publishing, highlighting compound A1's potential as a competitive ligand candidate owing to its better binding properties than the Standard.

4. Conclusion

This study successfully synthesized and characterized two novel Mannich base derivatives (S1 and S2), demonstrating their dual therapeutic potential as antibacterial and anticancer agents. FTIR and ^{1}H-NMR confirmed the formation of β-amino ketone structures. S2 exhibited enhanced antibacterial activity, likely due to its hydroxyl substituent, while S1 showed greater cytotoxic potency against MCF-7 cells, attributed to its methylated structure, enhancing cell membrane permeability. Molecular docking validated the pharmacological relevance of these compounds through strong interactions with key residues of the estrogen receptor alpha, supporting their therapeutic targeting potential. Scientifically, this research offers a well-integrated in vitro and in silico platform. However, the study lacks mechanistic validation of the observed bioactivities (e.g., apoptosis pathway activation or membrane disruption). Also, no toxicity or selectivity index was calculated. It would be beneficial to explore additional cell lines and Gram-negative strains, and to assess solubility and bioavailability parameters. Future work should involve in vivo pharmacokinetics, time-kill kinetics, ADMET profiling, and mechanistic studies such as Western blotting or flow cytometry. These results support the development of Mannich-based lead compounds for further drug development against resistant infections and hormone-dependent cancers.

REFERENCES

[1] P. Garg, J. Malhotra, P. Kulkarni, D. Horne, R. Salgia, and S. S. Singhal, "Emerging therapeutic strategies to overcome drug resistance in cancer cells," Cancers, vol. 16, no. 13, p. 2478, 2024.

[2] Tarin-Pello, B. Suay-Garcia, and M.-T. Perez-Gracia, "Antibiotic resistant bacteria: current situation and treatment options to accelerate the development of a new antimicrobial arsenal," Expert Rev. Anti-Infect. Ther., vol. 20, no. 8, pp. 1095-1108, 2022.

[3] S. K. Raju, P. Vengadhajalaphathy, R. Sundaram, S. Periyasamy, T. Chinnaraj, P. Sekar, "Recent advances in biological applications of mannich bases—An overview," Int. J. Pharm. Chem. Anal., vol. 10, no. 1, pp. 15-27, 2023.

[4] S. S. Raoof and A. S. Sadiq, "Mannich bases: Synthesis, pharmacological activity, and applications: A review," Iraqi J. Sci., vol. 2022, pp. 5086-5105.

[5] H. Nazir and M. M. Naseer, "The Isatin Scaffold: Exceptional Potential for the Design of Potent Bioactive Molecules," Synlett, 2025.

[6] M. Strzelecka, T. Glomb, M. Drąg-Zalesińska, J. Kulbacka, A. Szewczyk, J. Saczko, et al., "Synthesis, anticancer activity and molecular docking studies of novel N-Mannich bases of 1, 3, 4-oxadiazole based on 4, 6-dimethylpyridine scaffold," Int. J. Mol. Sci., vol. 23, no. 19, p. 11173, 2022.

[7] F. S. Tokalı, P. Taslimi, İ. H. Demircioğlu, K. Şendil, B. Tuzun, and İ. Gülçin, "Novel phenolic Mannich base derivatives: synthesis, bioactivity, molecular docking, and ADME-Tox studies," J. Iranian Chem. Soc., vol. 19, no. 2, pp. 563-577, 2022.

[8] M. Konus, D. Çetin, N. D. Kızılkan, C. Yılmaz, C. Fidan, M. Algso, et al., "Synthesis and biological activity of new indole based derivatives as potent anticancer, antioxidant and antimicrobial agents," J. Mol. Struct., vol. 1263, p. 133168, 2022.

[9] Z. H. Ali, D. Saleem, A. K. Abbas, B. S. Rasool, and M. S. Cheyad, "Synthesis and estimation of the insecticide and antibacterial activities for some new amide derivatives," Indonesian J. Chem., vol. 23, no. 6, pp. 1535-1541, 2023.

[10] H. K. Al-Ruba, "Synthesis, Antibacterial, and Anticancer Evaluation of Novel Imine Derivatives of 6-Aminopenicillins," Iraqi J. Biosci. Biomed., vol. 2, no. 1, pp. 150-170, 2025.

[11] Ajmal, A. Mahmood, C. Hayat, M. A. Hakami, B. S. Alotaibi, M. Umair, et al., "Computer-assisted drug repurposing for thymidylate kinase drug target in monkeypox virus," Front. Cell. Infect. Microbiol., vol. 13, p. 1159389, 2023.

[12] T. T. Eugene-Osoikhia, N. W. Odozi, E. O. Yeye, M. Isiaka, and I. A. Oladosu, "In-silico study of novel dimeric flavonoid (OC251FR2) isolated from the seeds of Garcinia kola Heckel (Clusiaceae) against alpha estrogen receptor (ER-α) of breast cancer," In Silico Pharmacol., vol. 12, no. 2, p. 108, 2024.

[13] T. Ehtezazi, K. Rahman, R. Davies, and A. G. Leach, "The pathological effects of circulating hydrophobic bile acids in Alzheimer's disease," J. Alzheimer's Dis. Rep., vol. 7, no. 1, pp. 173-211, 2023.

[14] T. Q. Sabah and S. R. Baqer, "Design, synthesis, and evaluation of some metal ion complexes of mannich base derived from 2-Mercaptobenzimidazole as potential antimicrobial agents," Iraqi J. Chem. Petroleum Eng., vol. 25, no. 3, pp. 115-125, 2024.

[15] T. Q. Manhee and A. J. Alabdali, "Synthesis, characterization and anticancer activity of Ni (II), Cu (II), Pd (II) and Au (III) complexes derived from novel Mannich base," Vietnam J. Chem., vol. 62, no. 2, pp. 201-210, 2024.

[16] M. A. Hameed and M. J. Al-Jeboori, "Synthesis, spectral characterization, DFT calculations, biological evaluation and molecular docking analysis of new Mannich compounds derived from cyclopentanone," J. Mol. Struct., vol. 1322, p. 140619, 2025.

[17] Z. H. Ali, N. R. Jber, and A. K. Abbas, Eds., "Synthesis and characterization of new 1, 3-oxazepine compounds from P-Phenylenediamine as insecticide (Aphidoidea)," in AIP Conf. Proc., AIP Publishing LLC, 2023, pp. 1-10.

[18] T. Rimpiläinen, A. Nunes, R. Calado, A. S. Fernandes, J. Andrade, E. Ntungwe, et al., "Increased antibacterial properties of indoline-derived phenolic Mannich bases," Eur. J. Med. Chem., vol. 220, p. 113459, 2021.